THE ROYAL SOCIETY

Instabilities and flame speeds in large-scale premixed gaseous explosions

By Derek Bradley

School of Mechanical Engineering, University of Leeds, Leeds LS2 9JT, UK

The instability of spherical flames in quiescent premixtures is considered using the linear theory developed by Bechtold & Matalon, which includes hydrodynamic and thermodiffusive instabilities. Ranges of unstable wavenumbers are presented for different Markstein numbers as the flame propagates, characterized by the flame Peclet number. Hydrodynamic instabilities arise at the larger wavelengths and cascade down through a range of ever-decreasing wavelengths to be stabilized at the smallest wavelength by thermodiffusive effects. It would appear that, in practice, the associated cell formation lags somewhat behind what is predicted by the theory and an attempt is made to allow for this. With it, a fractal analysis is employed with the two limiting unstable wavelengths as inner and outer cut-offs. The ever-increasing surface wrinkling as the flame propagates creates a larger surface area and consequent flame acceleration. The analysis yields an expression for the flame speed after a critical Peclet number has been attained. The flame speed increases as the square root of elapsed time and the analytical expression is in agreement with the results of measurements of large explosions. The fractal analysis is probably valid because of the large length-scales and small flame stretch rates, unlike those in many turbulent flames in engineering applications where the flame stretch rate usually reduces the burning rate. The mechanisms for the creation of turbulence are discussed, including a brief speculation of the repercussions for deflagration-to-detonation transitions in large-scale explosions, including supernovae.

Keywords: flame instabilities; large-scale explosions; deflagration–detonation transition; fractal flame analysis; Darrieus–Landau instability; thermodiffusive instability

1. Introduction

The storage and distribution of ever-increasing quantities of flammable gases create a potential hazard from large gaseous explosions in the atmosphere and a need to understand their nature. Experimental programmes have investigated such explosions (Lind & Whitson 1977; Gostintsev *et al*. 1988), which are unique in their large length-scales. A wide range of meteorological conditions can arise (Abdel-Gayed & Bradley 1982) and the associated turbulent parameters can be incorporated in mathematical models of turbulent combustion (Bradley *et al*. 1994) to predict turbulent burning velocities. The present study, however, concentrates on explosions in quiescent gas and the flame acceleration that arises from developing flame instabilities. Improved understanding of such very large deflagrations is also necessary for any

analysis of unconfined transitions to detonations, including those that possibly occur in supernovae (Khokhlov *et al*. 1997*a*).

The seminal studies of Darrieus (1938) and Landau & Lifshitz (1987) showed that the propagation at constant speed of a wave of density discontinuity creates a hydrodynamic instability. A flame advancing into unburned gas comprises such a surface. The instability may be explained, albeit simplistically, by considering the gas motion relative to the wave. When the unburned gas moves into the crest of a flame front it diverges and this increases the pressure. Conversely, the oncoming unburned gas converges as it approaches the trough of the flame front and this decreases the pressure. These pressure changes are fundamentally unstable, in that they increase the wrinkling of the flame front. As a consequence, the overall burning velocity also increases. The Darrieus–Landau model contains no characteristic length and its creators anticipated a much earlier development of turbulence than, in fact, occurs. Later, Istratov & Librovich (1966) showed that at least two characteristic length-scales were involved. It is now clear that, depending upon directional influences, thermodiffusive effects can either reduce or reinforce the hydrodynamic instability.

The combined influences of flame stretch and thermodiffusion are also important and their effects upon the laminar burning velocity, u_ℓ, of premixed gases are given by

$$\frac{u_\ell - u_n}{u_\ell} = KMa, \tag{1.1}$$

where u_ℓ is the burning velocity in the absence of stretch and u_n is that at the given stretch rate. When this stretch rate is normalized by the chemical time, δ_ℓ/u_ℓ, in which δ_ℓ is the flame thickness given by v/u_ℓ (v is the kinematic viscosity), it gives the Karlovitz stretch factor, K. Normalization of the Markstein length, also by δ_ℓ, gives the Markstein number, Ma, and the product of K and Ma gives the deficit in the burning velocity due to the flame stretch rate. The influences of thermodiffusion and activation energy, separately expressed in Lewis and Zeldovich numbers, are, together with the density ratio across the flame, all embodied in the Markstein number (Bradley *et al*. 1996).

When a flame surface becomes wrinkled by a perturbation a localized increase in curvature results in a localized increase in the stretch rate and K. This, with a positive value of Ma, *reduces* the burning velocity, while the associated *decrease* in curvature over a wavelength increases it and the perturbation is opposed. It is the mechanism by which thermodiffusive effects might stabilize a flame against the underlying Darrieus–Landau instability. If Ma is negative, the effects are reversed and the underlying aerodynamic instability is reinforced by thermodiffusive instability.

For simplicity, a spherical explosion flame is considered and it is shown how instabilities evolve first through the cracking of the flame surface, followed by the development of a cellular structure and, if the radius is large enough, the eventual appearance of a turbulent flame. Four regimes of flame propagation can be discerned, which, chronologically, involve: (i) stable laminar flame propagation; (ii) unsteady flame cracking and cell formation; (iii) cellular flame propagation; and (iv) self-turbulizing flame propagation. Transitions between these regimes are discussed principally in terms of the values of Peclet number, Pe (the mean flame radius normalized by δ_ℓ), and Markstein number of the mixture. The initial flame instability, together with its development as the flame propagates, is analysed. Eventually, the flame assumes many of the aspects of a turbulent flame.

2. Flame stability analysis

(*a*) *Growth of the instability*

The linear stability analysis of Bechtold & Matalon (1987) describes both the hydrodynamic and thermodiffusive influences upon the stability of an outwardly propagating spherical flame and provides the theoretical framework for the present work. The Markstein number is not used explicitly but, in terms of the notation of their paper, it can be shown to be

$$\frac{\gamma}{2\sigma}\left(\ell + \frac{2\sigma^2 \ln \sigma}{\gamma(\sigma - 1)}\right), \tag{2.1}$$

where σ is the density ratio of unburned to burned gas, γ is a function depending on σ and ℓ is the deviation of the Lewis number from unity on the scale of the activation energy ($\ell = 0$ when the diffusion of heat and mass balances). Distortions of the flame front are expressed relative to the basic spherical symmetry. Perturbed variables are expanded in spherical harmonic series and flame stability investigated with respect to all possible modes. After the flame of radius, r, has propagated beyond an initial value, r_0, significantly greater than δ_ℓ, the dimensionless amplitude, a, of the perturbation relative to the flame front, develops according to

$$a = a_0 R^{\omega(1+\Omega/Pe \ln R)}. \tag{2.2}$$

Here a_0 is the initial dimensionless amplitude of the perturbation, R is r/r_0, $Pe = r/\delta_\ell$ and ω is a growth-rate parameter dependent upon the density ratio, σ, while Ω depends upon both this and the Markstein number. Expressions for ω and Ω are given in terms of the series of spherical harmonic integers, n, by Bechtold & Matalon (1987) and by Bradley & Harper (1994). Typographical corrections to some key expressions in these references are given in the appendix.

The logarithmic growth rate, $\bar{A}$, of the amplitude of the perturbation with respect to the Peclet number depends on n and is derived from equation (2.2):

$$\bar{A}(n) = \frac{\mathrm{d}\ln(a/a_0)}{\mathrm{d}\ln Pe} = \omega\left(1 - \frac{\Omega}{Pe}\right). \tag{2.3}$$

A negative value of $\bar{A}(n)$ indicates a stable flame, a positive value an unstable one. On the right-hand side of the equation the first term, ω, gives the contribution to the growth rate of the Darrieus–Landau (DL) instability, while the second $(-\omega\Omega/Pe)$, gives the contribution due to thermodiffusive instability. These values and $\bar{A}(n)$ are shown for $\sigma = 6$ and different values of Ma and Pe as a function of n in figures 1–3. Consideration is confined to positive values of Ma. In figure 1, for $Ma = 1.4$, $Pe = 200$, interestingly, at small values of n the DL influence is stabilizing while the thermodiffusive influence is destabilizing. As n increases above 6 both components contribute to the instability and ω and $\bar{A}(n)$ become positive. The thermodiffusive contribution to instability, shown by the lower broken curve, is positive for all values of n and both instabilities combine to give a higher value of $\bar{A}(n)$. At higher values of Ma the value of $(-\omega\Omega/Pe)$ becomes negative and hence thermodiffusive effects now are stabilizing, as can be seen from figure 2, for $Ma = 4$ and $Pe = 300$. Here $\bar{A}(n)$ is everywhere negative and the flame is stable.

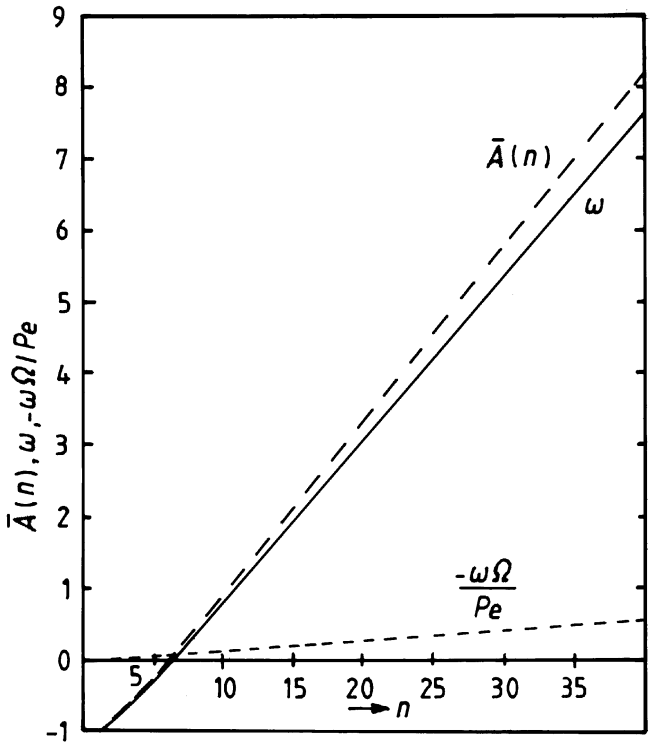

Figure 1. Logarithmic growth rate, $\bar{A}(n)$, of amplitude of perturbation, with DL, ω, and thermodiffusive $(-\omega\Omega/Pe)$ components as a function of n: $\sigma = 6$, $Ma = 1.4$, $Pe = 200$.

However, as the flame radius increases the stabilizing effect of flame stretch and thermodiffusion, measured by $(-\omega\Omega/Pe)$, decreases and at $Ma = 4$, $Pe = 600$ (figure 3), $\bar{A}(n)$ becomes positive over a range of values of n between 8 and 35. The Bechtold & Matalon (1987) theory resolves previous uncertainties about the existence of a limiting unstable upper value of n. One upper limit is imposed by the finite flame thickness, while in their numerical calculations of the DL instability Liberman *et al.* (1993) suggested the flame became stabilized at scales that exceeded δ_ℓ by at least an order of magnitude. In this present example this scale exceeds δ_ℓ by two orders of magnitude.

Between $Pe = 300$ and 600 for $Ma = 4$ (figures 2 and 3), there is a critical value of the Peclet number, Pe_c, and spherical harmonic, n_c, at which $\bar{A}(n)$ just becomes positive and the flame unstable. At values of Pe greater than Pe_c, as already noted for figure 3, the regime of instability is bounded by two values of n; the lower one will be defined by n_l, the upper one by n_s. The value of n where $\bar{A}(n)$ is a maximum is n_m. Values of Pe_c and n_c for $Ma = 2, 4$ and 8 are given in table 1.

(*b*) *Peninsular of instability*

For values of Ma between 2 and 8, where values of Pe_c could be computed, these values of n normalized by n_c can be generalized by plotting them against Pe/Pe_c, as in figure 4, for $\sigma = 6$. A peninsular of instability has a lower bound n_l/n_c and an

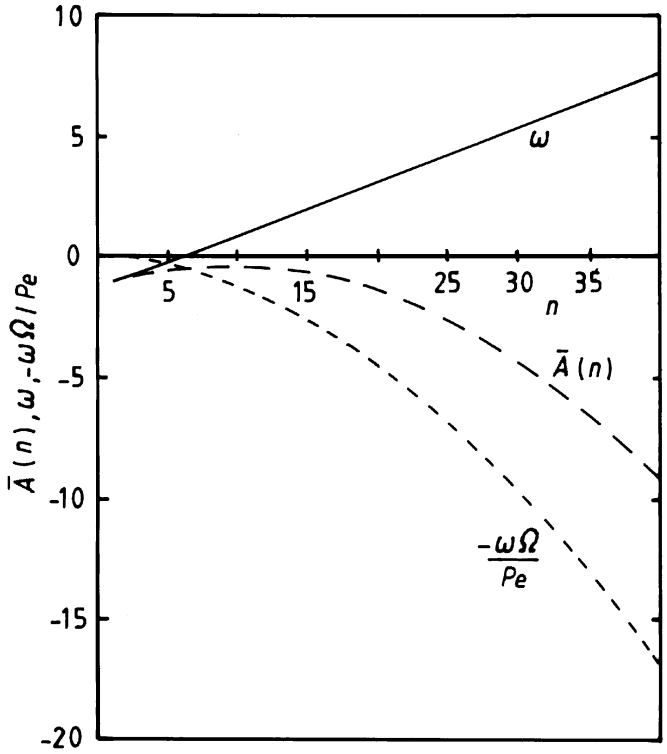

Figure 2. Logarithmic growth rate, $\bar{A}(n)$, of amplitude of perturbation, with DL, ω, and thermodiffusive $(-\omega\Omega/Pe)$ components as a function of n: $\sigma = 6$, $Ma = 4$, $Pe = 300$.

Table 1. *Values of* Pe_c *and* n_c *for* $\sigma = 6$

Ma	Pe_c	n_c
2	78.7	12.3
4	407	14.0
8	1062	14.5

upper bound n_s/n_c, while the middle curve gives values of n_m/n_c at which $\bar{A}(n)$ is a maximum.

A spherical harmonic, n, is essentially a wavenumber with an associated wavelength normalized by δ_ℓ that is indicated by Λ. These are related to Pe by (Bradley & Harper 1994)

$$n = \frac{2\pi Pe}{\Lambda}. \tag{2.4}$$

This wavenumber represents the number of wavelengths of a particular value around the flame circumference. The higher the value of n, the greater the potential number of cells on the flame surface. Instabilities are generated at the longer wavelengths, with a limiting lowest unstable wavenumber n_l, where the DL instability tends to be dominant. It can be seen from figure 4 that this wavenumber soon attains a constant

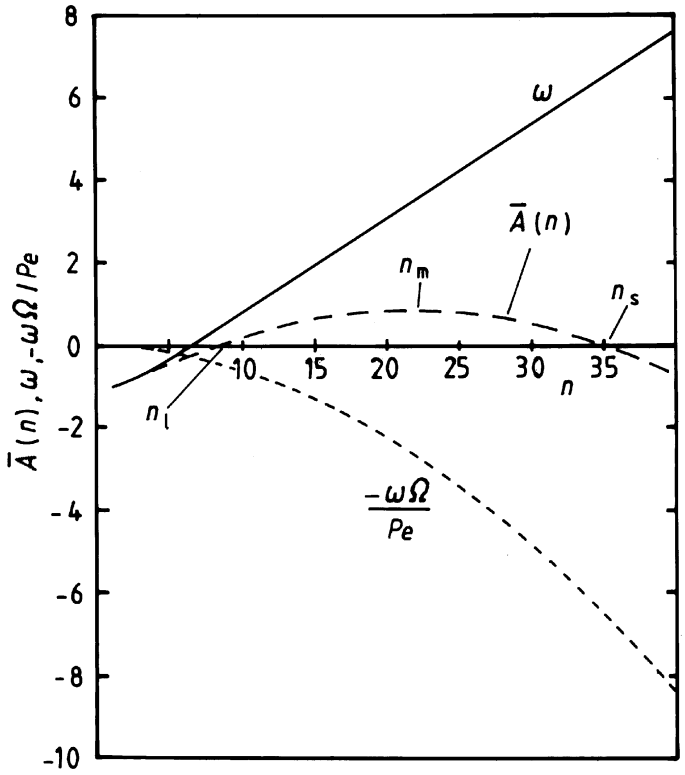

Figure 3. Logarithmic growth rate, $\bar{A}(n)$, of amplitude of perturbation, with DL, ω, and thermodiffusive $(-\omega\Omega/Pe)$ components as a function of n: $\sigma = 6$, $Ma = 4$, $Pe = 600$.

value that does not change as the flame propagates. It follows from equation (2.4) that the associated dimensionless longest unstable wavelength, Λ_l, must increase linearly with Pe. Figure 4 also shows that, in contrast, as the flame propagates the limiting value of the upper wavenumber, n_s, increases linearly with Pe and, from equation (2.4), the associated dimensionless smallest unstable wavelength, Λ_s, must be constant valued. This wavelength is associated with the stabilizing influence of thermodiffusion at high curvatures.

As the flame radius increases, so does the wavelength Λ_l. The flame stretch rate at these wavelengths is too small to stabilize the flame and further perturbations of shorter wavelength are created on the surface of the longer-wavelength perturbations. These too may be unstable and a cascade develops of progressively decreasing unstable wavelengths. The rate of growth of the amplitude of the instability is greatest at wavelengths that correspond to the wavenumber n_m. Eventually this cascade of ever-decreasing unstable wavelengths is terminated at the wavelength, Λ_s, where the flame stretch is sufficiently high to stabilize the flame. The cascade gives rise to a fractal-like flame wrinkling (Gostintstev *et al*. 1988; Filyand *et al*. 1994) and it can be argued that its fractal nature is similar to that of turbulence (Bradley 1992), but with an outer cut-off scale of Λ_l and an inner cut-off of Λ_s.

The ratio of the area of the fractal surface with this inner cut-off to that with a

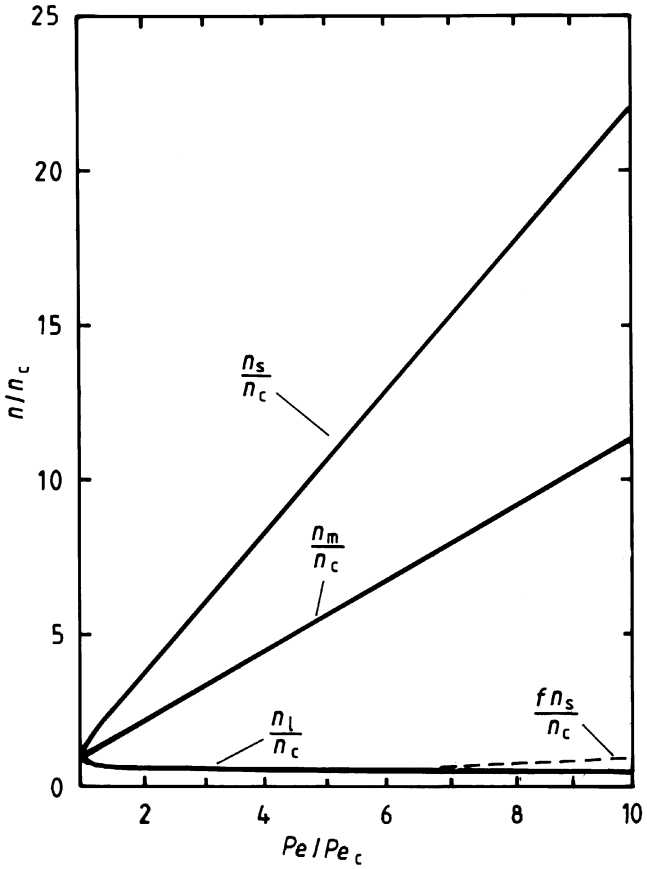

Figure 4. Normalized wavenumbers of lower and upper bounds of instability as a function of Pe/Pe_{c}; $n_{\mathrm{m}}/n_{\mathrm{c}}$ is a normalized wavenumber where $\bar{A}(n)$ is a maximum: $\sigma = 6$, $Ma = 2$, 4 and 8. Broken line gives $fn_{\mathrm{s}}/n_{\mathrm{c}}$ for $Pe_{\mathrm{cl}}/Pe_{\mathrm{c}} = 7$ and $f = 0.03$.

resolution given by the outer cut-off at a Peclet number of Pe is

$$\chi_{Pe} = \left(\frac{\Lambda_{\mathrm{l}}}{\Lambda_{\mathrm{s}}}\right)^{D-2} = \left(\frac{n_{\mathrm{s}}/n_{\mathrm{c}}}{n_{\mathrm{l}}/n_{\mathrm{c}}}\right)^{D-2}. \tag{2.5}$$

Different values have been proposed for the fractal dimension, D, of a wrinkled surface, but here a value of $\frac{7}{3}$ is taken (Bradley 1992). Shown in figure 5 are calculated values of $n_{\mathrm{m}}/n_{\mathrm{c}}$ and $n_{\mathrm{s}}/n_{\mathrm{c}}$ for different values of Pe/Pe_{c} and values of Ma of 2, 4 and 8, with $\sigma = 6$. Values of n_{l} are almost constant valued at about 6 or 7 over most of the range. It can be seen that the influence of Ma is small with this normalization.

If Pe is large enough for flame-stretch rates to be small, the ratio of the flame speed referred to the mean radius arising from the surface wrinkling, S, to the laminar flame speed of a smooth sphere, S_ℓ, is the ratio of the wrinkled to the smooth surface area:

$$\chi_{Pe} = \frac{S}{S_\ell} = \left(\frac{n_{\mathrm{s}}/n_{\mathrm{c}}}{n_{\mathrm{l}}/n_{\mathrm{c}}}\right)^{1/3}. \tag{2.6}$$

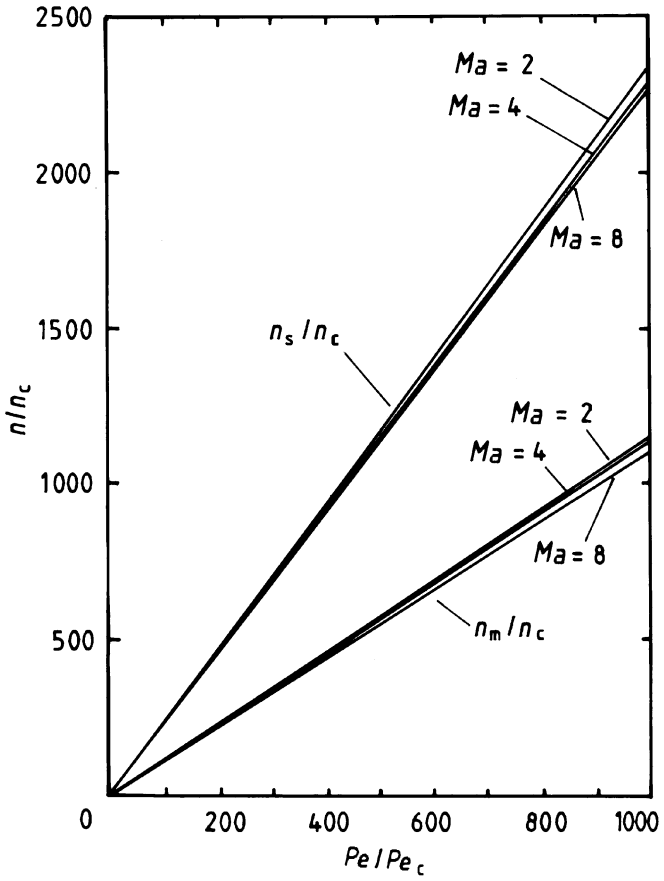

Figure 5. Normalized wavenumbers of upper bound of instability, n_s/n_c, and n_m/n_c as a function of Pe/Pe_c: $\sigma = 6$, $Ma = 2$, 4 and 8.

3. Regimes of spherical flame propagation

In the early stages of flame propagation just after ignition, $Pe \leqslant Pe_c$, the flame stretch rate, $2\,dr/r\,dt$, is sufficiently high to maintain flame stability and the flame surface is smooth. The burning velocity, u_n, is given by equation (1.1). As the flame propagates, eventually $Pe = Pe_c$, and the details of this transition have been studied by Bradley & Harper (1994) through analysis of high-speed schlieren cine photographs. They found that theoretical values of Pe_c, calculated as described above, were fairly close to the observed onset of instability provided this was defined by the start of crack propagation across the flame surface. The ways in which this instability develops are shown in detail in figure 6, drawn from actual cine frames (Lung 1986). A region of high negative curvature in the flame surface, typically arising from interaction with a spark electrode, initiates a propagating crack. Such cracks are prone to cross-cracking at corners, as shown in figure 6, until the cracks eventually form a coherent cellular structure covering the entire flame surface. The linear theory of Bechtold & Matalon (1987) cannot predict such structural development, but Kuznetsov & Minaev (1996) have attempted to do this numerically

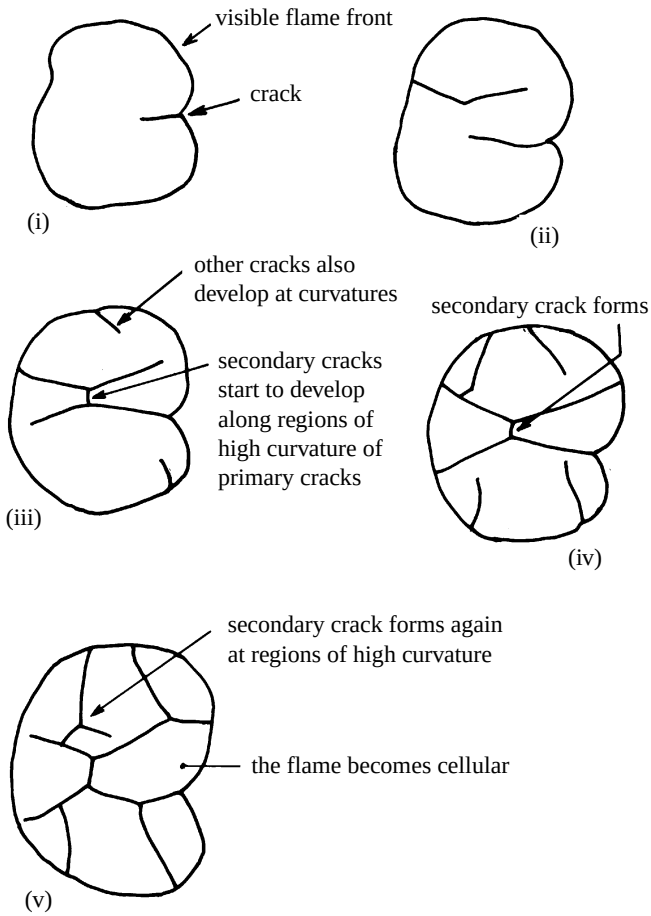

Figure 6. Details of crack development on a flame surface (Lung 1986).

using Sivashinky's (1977, 1983) model of flame surface development. They suggest the cracks originate at the longer wavelengths and demonstrate how the boundaries of separate cells form a complete web of cracks, in qualitative agreement with the experimental observations of Bradley & Harper (1994).

It would appear, however, that the creation of new cells cannot keep pace with the growth of the flame kernel. As the flame expands experiments show the area of individual cells also increases until, eventually, at a second critical Peclet number, Pe_{cl}, smaller cells are created. This first occurrence of a developed cellular structure is accompanied by an increase in flame speed, as a result of the increase in flame surface area. The creation of cells can only occur when the localized flame stretch of the cell surface is sufficiently reduced to allow the growth of an instability of shorter wavelength. For values of $Pe \geqslant Pe_{\mathrm{cl}}$ the flame speed increases continuously as a consequence of the increasingly wrinkled flame surface area. The shortest wavelength in the cascade is that associated with stabilization of the LD instability by thermodiffusive effects.

The growth of cells until they subdivide to form more stable and highly stretched smaller cells is a dynamic process in which the growth of instabilities appears to

lag behind the theoretical predictions of Bechtold & Matalon (1987). A time lag in the development of low-wavelength stabilized cells is suggested by the values of Pe_{cl} measured by Groff (1982) for propane–air explosions. These are between 10 and 20 times greater than the corresponding value of Pe_{c} (Bradley & Harper 1994). Furthermore, Groff (1982) could detect no significant change in flame speed just after the development of the cellular structure. Values of $Pe_{\mathrm{cl}} \geqslant Pe_{\mathrm{c}}$ have also been observed in iso-octane–air and methane–air explosions over a wide range of pressures and temperatures and correlated by Bradley *et al.* (1998) and Gu *et al.* (2000) by

$$Pe_{\mathrm{cl}} = 177Ma + 2177. \tag{3.1}$$

As Pe increases beyond Pe_{cl}, the range of unstable wavelengths increases linearly with Pe, until it becomes similar to that in turbulent flow. Gostintsev *et al.* (1988) surveyed the results of experimental measurements of flame propagation in large-scale explosions and suggested a critical Peclet number, between about 120 000 and 220 000, for a transition to a turbulent flame. In every case the burning velocity is about three times the laminar burning velocity just after the suggested transition (Bradley 1997). The nature of combustion in the regime where $Pe \geqslant Pe_{\mathrm{cl}}$ is now discussed in more detail.

4. Influence of flame instability on flame speed

To account for the time lag in the development of instabilities the cut-off wavenumber of the shorter wavelength is empirically reduced by taking the datum Peclet number for the onset of instability, cell formation and flame acceleration to be Pe_{cl}, rather than Pe_{c}. This procedure is illustrated in figure 4 for $Pe_{\mathrm{cl}}/Pe_{\mathrm{c}} = 7$. The new peninsular of instability is bounded by the upper broken line, $fn_{\mathrm{s}}/n_{\mathrm{c}}$, where f is a constant, less than unity, and the lower unmodified $n_{\mathrm{l}}/n_{\mathrm{c}}$ line. This procedure both increases the wavelength of the inner cut-off and also provides a better Peclet number datum, in that it is at Pe_{cl} that the increase in flame speed due to wrinkling begins. Conditions at this second critical Peclet number, $f(n_{\mathrm{s}}/n_{\mathrm{c}})_{\mathrm{cl}} = (n_{\mathrm{l}}/n_{\mathrm{c}})_{\mathrm{cl}}$, define the value of f. As a consequence, the previous expression for flame speed ratio (equation (2.6)) becomes, for $Pe \geqslant Pe_{\mathrm{cl}}$,

$$\frac{S}{S_\ell} = \left(\frac{fn_{\mathrm{s}}/n_{\mathrm{c}}}{n_{\mathrm{l}}/n_{\mathrm{c}}}\right)^{1/3}. \tag{4.1}$$

Because

$$S_\ell = \sigma u_\ell \quad \text{and} \quad S = r_{\mathrm{c}}\frac{\mathrm{d}Pe/Pe_{\mathrm{c}}}{\mathrm{d}t},$$

where r_{c} is the dimensional radius corresponding to Pe_{c} and t is time,

$$\frac{\mathrm{d}Pe/Pe_{\mathrm{c}}}{\mathrm{d}t} = \left(\frac{\sigma u_\ell}{r_{\mathrm{c}}}\right)\left(\frac{fn_{\mathrm{s}}/n_{\mathrm{c}}}{n_{\mathrm{l}}/n_{\mathrm{c}}}\right)^{1/3}. \tag{4.2}$$

In the regime of developed cellular flame wrinkling $(n_{\mathrm{s}}/n_{\mathrm{c}})$ increases linearly with (Pe/Pe_{c}) (see figure 5), and $n_{\mathrm{l}}/n_{\mathrm{c}}$ soon becomes constant valued. Hence

$$\frac{\mathrm{d}(Pe/Pe_{\mathrm{c}})}{\mathrm{d}t} = \left(\frac{\sigma u_\ell}{r_{\mathrm{c}}}\right)\left[\left(\frac{n_{\mathrm{c}}}{n_{\mathrm{l}}}\right)\frac{\mathrm{d}(fn_{\mathrm{s}}/n_{\mathrm{c}})}{\mathrm{d}(Pe/Pe_{\mathrm{c}})}\left(\frac{Pe}{Pe_{\mathrm{c}}} - \frac{Pe_{\mathrm{cl}}}{Pe_{\mathrm{c}}}\right) + \left(\frac{fn_{\mathrm{s}}}{n_{\mathrm{c}}}\right)_{\mathrm{cl}}\left(\frac{n_{\mathrm{c}}}{n_{\mathrm{l}}}\right)\right]^{1/3}. \tag{4.3}$$

Let

$$\left(\frac{n_c}{n_l}\right) f\left(\frac{\mathrm{d}(n_s/n_c)}{\mathrm{d}(Pe/Pe_c)}\right) = \kappa = \text{const.}$$

Hence

$$\frac{\mathrm{d}(Pe/Pe_c)}{\left[\kappa\left(\dfrac{Pe}{Pe_c} - \dfrac{Pe_{cl}}{Pe_c}\right) + \left(\dfrac{n_c}{n_l}\right) f\left(\dfrac{n_s}{n_c}\right)_{cl}\right]^{1/3}} = \left(\frac{\sigma u_\ell}{r_c}\right) \mathrm{d}t. \tag{4.4}$$

Integration gives

$$Pe = Pe_{cl} - \left(\frac{n_c}{n_l}\right)\frac{f}{\kappa}\left(\frac{n_s}{n_c}\right)_{cl} Pe_c + \left\{\frac{2}{3}\left(\frac{\sigma u_\ell^2}{v Pe_c^{1/3}}\right)\kappa^{1/3} t\right\}^{3/2} \tag{4.5}$$

provided

$$t = 0 \quad \text{when } Pe = Pe_{cl} - \left(\frac{n_c}{n_l}\right)\frac{f}{\kappa}\left(\frac{n_s}{n_c}\right)_{cl} Pe_c.$$

In terms of the dimensional radius, r,

$$r = r_0 + \left[\frac{0.544\sigma^{3/2} u_\ell^2 \kappa^{1/2}}{v^{1/2} Pe_c^{1/2}}\right] t^{3/2}, \tag{4.6}$$

where

$$r_0 = r_{cl} - \left(\frac{n_c}{n_l}\right)\frac{f}{\kappa}\left(\frac{n_s}{n_c}\right)_{cl} r_c. \tag{4.7}$$

Gostintsev *et al.* (1988) have generalized the experimental data on large-scale turbulent explosions empirically in the form

$$r = r_{0G} + A_G t^{3/2}, \tag{4.8}$$

where A_G is an experimentally determined constant that depends upon the fuel–air mixture and r_{0G} is a datum flame radius. Provided Ma is known, the present analytical approach in conjunction with equation (3.1) enables the bracketed terms in equation (4.6), A, to be evaluated and compared with the corresponding experimental value of A_G, reported by Gostintsev *et al.* (1988). The results for three diverse mixtures, for which the value of Ma is known with sufficient accuracy, are given in table 2. In every case, values of A are greater than those of A_G. One explanation of this is that the theory takes no account of radiative loss from the flame kernel. This might explain up to *ca.* 20% of the discrepancy.

Differentiation of equation (4.6) gives the flame speed

$$S = \frac{\mathrm{d}r}{\mathrm{d}t} = \tfrac{3}{2} A t^{1/2}, \tag{4.9}$$

and also, from equation (4.6),

$$S = \tfrac{3}{2} A^{2/3} (r - r_0)^{1/3}. \tag{4.10}$$

Table 2. *Comparison of computed values of A (the bracketed term in equation (4.6)) with experimental values of A_G from (Gostintsev et al. 1988) (SI units)*

mixture	σ	u_ℓ	Ma	$v \times 10^5$	Pe_c	f	A	A_G
10% CH_4–air	7.456	0.385	4.02	1.574	414.2	0.0309	8.04	5.7
4% C_3H_8–air	7.915	0.38	5.0	1.726	598.5	0.0431	8.13	7.1
36.4% H_2–air	6.673	2.75	12	2.36	1782	0.1071	275	166

This implied continuing flame acceleration raises the possibility of a deflagration-to-detonation transition. The gas velocity just ahead of the flame is $S(\sigma-1)/\sigma$ and for such a transition this must first attain the acoustic velocity. For the most reactive hydrogen–air mixture in table 2 a gas velocity of $330\,\mathrm{m\,s^{-1}}$ would be reached at a flame radius of 230 m, neglecting radiation. This confirms the conclusion of other analyses that such transitions are much more difficult in unconfined than in confined explosions (Khokhlov *et al.* 1997*b*).

Further developments of Sivashinsky's (1977, 1983) equation for the evolution of a flame surface have led to more comprehensive direct numerical simulations. Those of Filyand *et al.* (1994) give a satisfactory qualitative description of the flame wrinkling and the dependency of S upon $t^{1/2}$, but generally such simulations tend to underestimate the flame speed. There are difficulties in the numerical processing of the strongly nonlinear equations and the non-steady cellular structure. Cambray *et al.* (1996) have suggested that as the flame Peclet number exceeds the critical value the theoretical understanding deteriorates, particularly in regard to the causes of cell splitting. This affects the flame speed and these researchers have developed a mean-field approach based upon the dynamics of poles to describe the wrinkle crests. In another approach, Ashurst (1997) uses two-dimensional Lagrangian simulations and a potential flow assumption to derive an expression with several similarities to equation (4.6), again confirming the $t^{1/2}$ dependency of S.

5. Discussion

The principal difference between the present study and that of Gostintsev *et al.* (1988) is that, in the former, equation (4.6) applies when $Pe \geqslant Pe_{cl}$, whereas, in the latter, equation (4.8) only applies above much higher critical Peclet numbers of about 150 000 and is associated by these workers with a sharp transition to a turbulent flame. Turbulence is characterized by velocity fluctuations that extend over a range of wavelengths. When this range is of a sufficient extent the flow is described as turbulent. For isotropic turbulence, the power spectral density function exhibits an inertial subrange that extends over a range of about one decade of wavenumbers when the Reynolds number based on the Taylor scale attains a value of about 100. This is probably close to a lower limit of Reynolds number that characterizes the onset of turbulence. A comparable range of unstable wavelengths can arise in spherical explosions between n_e/n_c and fn_s/n_c. This extends over a decade at about $Pe/Pe_c = 64$ for $Pe_{cl}/Pe_c = 7$ and $f = 0.03$ (see figure 4). For Peclet numbers higher than this the flame therefore might possibly be classed as turbulent, but it is difficult to identify a sharp transition with any certainty. Furthermore, the turbulence is characterized,

not by an external flow, but by a self-generation mechanism inherent in the flame structure.

The large length-scales in atmospheric explosions create not only the possibility of a wide range of unstable wavelengths, but also of low values of flame stretch rate. This contrasts with the turbulent combustion in most engineering applications, where length-scales are small. As a consequence of this, and the often high flow rates, the flame stretch rates in these applications can reduce turbulent burning velocities well below values suggested by, sometimes invalid, simple fractal analysis (Bradley 1992). The fact that the present combination of instability and fractal analyses seems to be in satisfactory agreement with experiment tends to confirm the absence of strong flame stretch rate effects. This is supported by the extended Borghi diagram of turbulent flame regimes (Abdel-Gayed & Bradley 1985). Reference to this shows that at high values of turbulent length-scale, normalized by δ_ℓ, high values of turbulent burning velocity, normalized by u_ℓ, can be achieved at rather low values of RMS turbulent velocity, normalized by u_ℓ, and very low values of Karlovitz stretch factor. In the present large-scale explosions, the turbulent length-scale normalized by δ_ℓ might be taken as Λ_ℓ, and because $n_1 \approx 2\pi$, from equation (2.4), $\Lambda_\ell \approx Pe$, giving potentially very high normalized turbulent length-scales.

There remains the question of the mechanism for the generation of the turbulence, because in the theory of Bechtold & Matalon (1987), although the disturbances in the unburned gas are caused by the distortion of the flame front, the unburned gas retains its irrotational structure. In practice, the most probable sources of turbulence are Taylor instabilities arising from the baroclinic vorticity-generation term, $\nabla p \times \nabla\rho/\rho^2$, in the vorticity equation (Bradley & Harper 1994). Both gravity and the hydrodynamic pressure contribute to the pressure term. Bray *et al.* (1981) have shown theoretically how, in unconfined flames, turbulence increases through the flame as a result of buoyant production of turbulence and this same mechanism, associated with the mean pressure gradient, also causes counter-gradient diffusion. Using particle image velocimetry, Mueller *et al.* (1998) have shown flame-generated vorticity to be favoured by buoyancy-driven flames, large eddy scales, low turbulence, low Karlovitz stretch factors and an upward flow of products. These theoretical and experimental findings confirm that the turbulence in large-scale explosions can be flame generated. There is also evidence that the very large length-scale turbulence in supernovae is driven by buoyancy (Khokhlov *et al.* 1997*a*).

6. Conclusions

(1) The instability theory of Bechtold & Matalon (1987) is able to express the wavenumbers at which a spherical flame is unstable in terms of Markstein number and density ratio for different Peclet numbers. Critical Peclet numbers can be identified for the onset of instability.

(2) The structure of cellular flames resulting from the instabilities becomes fractal in nature. The instabilities originate as a Darrieus–Landau instability at the longer wavelengths and cascade to the shortest wavelength, to be stabilized by thermodiffusive instability. An individual cell grows in size as the flame propagates and its curvature diminishes, with the result that the local stretch rate decreases to the point at which the cell is locally destabilized, with the formation of smaller cells of higher curvature.

(3) Experiments suggest there is a time lag in cell formation, such that the actual critical Peclet number for developed cellularity is larger than that for the onset of instability.

(4) From these findings, with the limits of unstable wavelengths as outer and inner cut-offs, a fractal expression gives the increase in surface area as a result of flame wrinkling due to instabilities. At the low flame stretch rates that seem to obtain, this increase in surface area gives a corresponding increase in flame speed. The expression for this shows the flame speed to depend on $t^{1/2}$ and is in satisfactory agreement with experimental measurements.

(5) The expression for flame speed enables the radius at which an acoustic velocity is attained to be found. This shows that very large radii are necessary to obtain a deflagration-to-detonation transition in unconfined flames in a quiescent mixture.

(6) The mechanisms for flame-generated turbulence have been discussed and these are favoured in large-scale unconfined explosions.

Appendix A.

In Bechtold & Matalon (1987) the expressions for Q_1 and Q_2 following eqn (52) on p. 85 must be replaced by the following expressions:

$$Q_1 = [2\omega a + b - 2a]^{-1}\left\{\frac{\ln\sigma}{\sigma-1}[(\sigma+1)n^4 + (2\omega+5)\sigma n^3 + (\omega\sigma - 2\sigma^2 + \sigma - 1)n^2 + (\sigma - 7 - 3\omega - \sigma\omega)n\sigma - 2\sigma(1+\omega)] + n(n^2-1)(n+2)\frac{\sigma-1}{\sigma}\right\}, \quad \text{(A 1)}$$

$$Q_2 = \gamma[2\sigma(2\omega a + b - 2a)]^{-1}\{2n^4 + [2\omega\sigma + 2\omega + 10\sigma - 3]n^3 + [2\sigma\omega^2 + (5\sigma-1)\omega + 3\sigma - 2\sigma^2 - 2]n^2 + [\sigma\omega^2(1-4\sigma) - (14\sigma^2+1)\omega + 3 - 9\sigma - 8\sigma^2]n - 2\sigma(\omega^2 + 4\omega + 3)\}. \quad \text{(A 2)}$$

In Bradley & Harper (1994), a multiplying n must be inserted after $(4 + 5\sigma)$ in the expression for b in equation (A2) on p. 570.

References

Abdel-Gayed, R. G. & Bradley, D. 1982 The influence of turbulence upon the rate of turbulent burning. In *Fuel–air explosions* (ed. J. H. S. Lee & C. M. Guirao), pp. 51–68. University of Waterloo.

Abdel-Gayed, R. G. & Bradley, D. 1985 Criteria for turbulent propagation limits of premixed flames. *Combust. Flame* **62**, 61–68.

Ashurst, W. T. 1997 Darrieus–Landau instability, growing cycloids and expanding flame acceleration. *Combust. Theory Modelling* **1**, 405–428.

Bechtold, J. K. & Matalon, M. 1987 Hydrodynamic and diffusion effects on the stability of spherically expanding flames. *Combust. Flame* **67**, 77–90.

Bradley, D. 1992 How fast can we burn? In *Twenty-fourth Symp. (Int.) on Combustion*, pp. 247–262. Pittsburgh, PA: The Combustion Institute.

Bradley, D. 1997 Evolution of flame propagation in large diameter explosions. In *Proc. 2nd Int. Seminar on Fire and Explosion Hazard of Substances and Venting of Deflagrations* (ed. V. Molkov). Moscow: All-Russian Research Institute for Fire Protection.

Bradley, D. & Harper, C. 1994 The development of instabilities in laminar explosion flames. *Combust. Flame* **99**, 562–572.

Bradley, D., Gaskell, P. H. & Gu, X. J. 1994 Application of a Reynolds stress, stretched flamelet, mathematical model to computations of turbulent burning velocities and comparison with experiments. *Combust. Flame* **96**, 221–248.

Bradley, D., Gaskell, P. H. & Gu, X. J. 1996 Burning velocities, Markstein lengths, and flame quenching for spherical methane–air flames: a computational study. *Combust. Flame* **104**, 176–198.

Bradley, D., Hicks, R. A., Lawes, M., Sheppard, C. G. W. & Woolley, R. 1998 The measurement of laminar burning velocities and Markstein numbers for iso-octane–air and iso-octane-*n*-heptane–air mixtures at elevated temperatures and pressures in an explosion bomb. *Combust. Flame* **115**, 126–144.

Bray, K. N. C., Libby, P. A., Masuya, G. & Moss, J. B. 1981 Turbulence production in premixed turbulent flames. *Combust. Sci. Technol.* **25**, 127–140.

Cambray, P., Joulain, K. & Joulin, G. 1996 Coalescence problems in the theory of expanding wrinkled premixed flames. *Combust. Sci. Technol.* **112**, 271–299.

Darrieus, G. 1938 Propagation d'un front de flamme: assai de théorie des vitesses anomales de déflagration par developpement spontané de la turbulence. Presented at *6th Int. Cong. Appl. Mech. 1946, Paris*.

Filyand, L., Sivashinsky, G. I. & Frankel, M. L. 1994 On self-acceleration of outward propagating wrinkled flames. *Physica* D **72**, 110–118.

Gostintsev, Yu. A., Istratov, A. G. & Shulenin, Yu. V. 1988 Self-similar propagation of a free turbulent flame in mixed gas mixtures. *Combust. Explosion and Shock Waves* March, pp. 563–569. (Translated from *Fizika Gorenyiya i Vzryva* (1988) **24**(5), 63–70.)

Groff, E. G. 1982 The cellular nature of confined spherical propane–air flames. *Combust. Flame* **48**, 51–62.

Gu, X. J., Haq, M. Z., Lawes, M. & Woolley, R. 2000 Laminar burning velocity and Markstein length measurements for methane–air mixtures. *Combust. Flame*. (In the press.)

Istratov, A. G. & Librovich, V. B. 1966 The influence of transport processes on the stability of a plane flame front. *Prikl. Mat. Mekh.* **30**, 451–466.

Khokhlov, A. M., Oran, E. S. & Wheeler, J. C. 1997*a* Deflagration-to-detonation transition in thermonuclear supernovae. *Astrophys. Jl* **478**, 678–688.

Khokhlov, A. M., Oran, E. S. & Wheeler, J. C. 1997*b* A theory of deflagration-to-detonation transition in unconfined flames. *Combust. Flame* **108**, 503–517.

Kuznetsov, E. A. & Minaev, S. S. 1996 Formation and propagation of cracks on the flame surface. *Phys. Lett.* A **221**, 187–192.

Landau, L. D. & Lifshitz, E. M. 1987 *Fluid mechanics*. Oxford: Pergamon.

Liberman, M. A., Bychkov, V. V. & Goldberg, S. M. 1993 *Zh. Eksp. Teor. Fiz.* **104**, 2685.

Lind, C. D. & Whitson, J. C. 1977 Explosive hazards associated with spills of large quantities of hazardous materials. Phase II. Report no. CG-D-85-77, Department of Transportation, United States Coast Guard.

Lung, F. K.-K. 1986 PhD thesis, University of Leeds.

Mueller, C. J., Driscoll, J. F., Reuss, D. L., Drake, M. C. & Rosalik, M. E. 1998 Vorticity generation and attenuation as vortices convect through a premixed flame. *Combust. Flame* **112**, 342–358.

Sivashinsky, G. I. 1977 Nonlinear analysis of hydrodynamic instability in laminar flames. Part I. Derivation of basic equations. *Acta. Astronaut.* **4**, 1177–1206.

Sivashinsky, G. I. 1983 Instabilities, pattern formation and turbulence in flames. *A. Rev. Fluid Mech.* **15**, 179–199.